Biosensors and Bioelectronics 85 (2016) 698–706

Contents lists available at ScienceDirect

Biosensors and Bioelectronics

journal homepage: www.elsevier.com/locate/bios

Electrochemical immunosensor constructed using TiO_2 nanotubes as immobilization scaffold and tracing tag

Xiaohe Huo [a], Peipei Liu [a], Jie Zhu [a], Xiaoqiang Liu [a,*], Huangxian Ju [b,**]

[a] Institute of Environmental and Analytical Sciences, College of Chemistry and Chemical Engineering, Henan University, Kaifeng, Henan Province 475004, PR China

[b] State Key Laboratory of Analytical Chemistry for Life Science, Department of Chemistry, Nanjing University, Nanjing 210023, PR China

ARTICLE INFO

Article history:
Received 22 December 2015
Received in revised form
3 March 2016
Accepted 17 May 2016
Available online 18 May 2016

Keywords:
Immunosensor
TiO_2 nanotube
Polyaniline
α-fetoprotein
Protein G′

ABSTRACT

A ternary TiO_2 nanotube (TNT) composite and a signal antibody and horseradish peroxidase (HRP) functionalized TNT were designed as an electrode scaffold for immobilization of high quantity of capture antibody and a tracing tag for immunosensing, respectively. The polyaniline (PANI) was coated on TNTs by chemical oxidative polymerization, and gold nanoparticles were deposited on TNT-PANI with a routine chemical reduction. Various techniques including scanning electron microscopy, energy dispersive X-ray, transmission electron microscope, X-ray diffraction, Fourier transform infrared spectra, X-ray photoelectron spectra, impedance and electrochemical techniques were used to characterize the nanomaterials. Using bis(sulfosuccinimidyl) suberate as amino cross-linker, the TNT composite could be further functionalized with protein G′ for oriented immobilization of capture antibody on electrode surface. Upon sandwich-type immunoreaction, the signal antibody on the tracing tag was quantitatively captured on the surface to generate sensitive electrochemical response with a H_2O_2 mediated HRP catalytic reaction. With α-fetoprotein as an analyte model, the immunosensor showed a linear range of 0.01–350 ng mL^{-1} with a detection limit of 1.5 pg mL^{-1}. The accelerated electron transfer by the ternary composite, oriented immobilization of capture antibody and high loading of HRP on the TNT tracing tag greatly amplified the electrochemical signal, and led to the superior performance of the immunoassay.

1. Introduction

Electrochemical immunoassay not only exhibits the advantages of the electrochemical detection including high sensitivity, economic and rapidity, but also possesses high selectivity and specificity of the immunological recognition (Pinwattana et al., 2010). The excellent selectivity and strong interaction between antibody and antigen allow electrochemical immunosensors to be employed for the determination of biomolecules in complex biological matrices such as blood, plasma or urine (Ekins, 1999; Meusel et al., 1995). Compared with label-free immunosensors, the labeled immunosensors use signal-generating labels to achieve more sensitive and versatile detection. Accordingly, numbers of enzymes such as horseradish peroxidase (HRP), glucose oxidase and alkaline phosphatase have been frequently used as immunosensor labels to amplify the detection signal (Luppa et al., 2001). These labeled immunosensors have been extensively used for sensitive and accuracy detection of tumor markers, which plays key roles in early prediction, diagnosis and treatment of cancers (Kavosi et al., 2014). For instance, α-fetoprotein (AFP), an oncogenic plasma glycoprotein mainly produced from the liver, yolk sac and gastrointestinal tract of fetal human (Maeng et al., 2008), has been extensively studied as the clinical tumor biomarker for liver cancer diagnosis with a cut-off concentration of 25 ng mL^{-1} (Liu et al., 2015; Xu et al., 2015). Accordingly, different techniques including quartz crystal microbalance (Chou et al., 2002), surface plasmon resonance (Chang et al., 2009), electrochemical immunosensor (Wang et al., 2009), chemiluminescence assay (Qin et al., 2012), and enzyme-linked immunosorbent assay (Paradela and Albar, 2008) etc have been developed to detect AFP. Among these immunoassay methods, electrochemical immunosensors have been demonstrated to be the most efficient, fast, economic and sensitive detection device.

With the rapid development of nanotechnology, various nanomaterials such as carbon (F. Li et al., 2015; Liu et al., 2011), graphene (P. Li et al., 2015), quantum dots (Xu et al., 2015) and noble metals (N. Li et al., 2015; Qi et al., 2014) etc have been widely used as immobilization scaffolds for preparation of biosensors.

* Corresponding author.
** Corresponding author.
E-mail addresses: liuxiaoqiang@henu.edu.cn (X. Liu), hxju@nju.edu.cn (H. Ju).

http://dx.doi.org/10.1016/j.bios.2016.05.053
0956-5663/

Among them, TiO_2 nanomaterials have been paid special attention due to their inherent advantages including large surface area, high stability, facile and environment friendly synthesis, non-toxicity and tunable size (Song et al., 2012; Zhao et al., 2014). For example, a label-free voltammetric immunosensor based on bipyridinium dibromide functionalized TiO_2 nanoparticles has been developed (Liang et al., 2008). The immunosensor exhibits a wide linear range from 1.25 to 200 ng mL^{-1} with a detection limit of 0.6 ng mL^{-1} for AFP due to the prominent biocompatibility, good electron transfer ability and excellent adsorption capability of TiO_2 composite. Due to high ratio of surface to volume, excellent biocompatibility and special geometry (porous structure), TiO_2 nanotube can be used as an excellent carrier for quantitative loading of tracer enzymes and signal antibodies to amplify the enzymatically catalytic signal, which leads to highly sensitive electrochemical immunoassay. However, the hydrothermally synthesized TiO_2 nanomaterials have seldom been applied in the immunoassay probably because of their poor conductivity and surface inertness, which is not advantageous to the immobilization of biomoleclues. Therefore, it is necessary and meaningful to find a new way for stable immobilization of biomolecules on TiO_2 nanomaterials. Suberic acid bis(3-sulfo-N-hydroxysuccinimide ester) sodium salt (BS^3) is a bifunctional cross-linker with the properties of water solubility, non-cleavability and membrane impermeability (Thamake et al., 2011). Its terminal amino reactive groups (N-hydroxysuccinimide ester) can readily couple to any molecules containing primary amines by amide bonds (Staros, 1982). Protein G′ produced by genetically engineered truncation of protein G retains the affinity of protein G for IgG (Goward et al., 1990) but lacks albumin, bio-membrane and Fab fragment binding sites (Fowler et al., 2007). Therefore, it can be effectively applied for the oriented immobilization of antibodies through their non-antigenic (Fc) regions. This work used BS^3 as an effective cross-linking reagent and protein G′ as a binding mediator to achieve the oriented immobilization of capture antibody on TNT composite modified electrode surface.

In order to introduce amino groups on TNT surface and improve the conductivity of the TNT composite, this work firstly formed a polymer of aniline on TNT, and deposited AuNPs on PANI|TNT to obtain an AuNPs|PANI|TNT composite. The positively charged amino groups of PANI could electrostatically attract $AuCl_4^-$ to facilitate the deposition of AuNPs. Moreover, both PANI and AuNPs improved the electrical conductivity of TNT and biocompatibility. After using chitosan to anchor the ternary composite on the electrode, protein G′ was immobilized on the ternary composite for convenient immobilization of capture antibody. At the same time, signal antibody and HRP were also immobilized on amino-functionalized TNTs with BS^3 to form a tracing tag. The proposed immunosensor showed a wide linear range with a pg mL^{-1}-leveled detection limit. Thus this provided a new avenue for functionalization of TNT with biomolecules and its application in immunosensing.

2. Experimental

2.1. Material and reagents

Mouse monoclonal capture and signal anti-AFP antibodies (clone no. A14C11 and A46C9) and AFP ($\geq$96%) (Product no. A0101) were purchased from Shuangliu Zhenglong Biochem. Lab (Chengdu, China) and were immediately diluted to required concentrations with 0.02 M phosphate buffer (pH 7.4) before use. TiO_2 nanoparticles (P25) were purchased from Tianjin Chemical Reagent Co., Ltd., China. 3-Aminopropyltriethoxysilane (APTES), BS^3, HRP, bovine serum albumin (BSA), gold (III) chloride trihydrate ($HAuCl_4 \cdot 3H_2O$), protein G′ from proprietary source and chitosan (CS, 85% deacetylation) were all ordered from Sigma-Aldrich Chemical Co. (St. Louis, MO). Aniline monomer (99.5%), ammonium persulfate (APS, 98%), hydroquinone and ammonia (28%) were obtained from J&K Scientific Ltd. (Beijing, China). Trisodium citrate, 30% H_2O_2 (v/v), sodium borohydride ($NaBH_4$) were obtained from Sinopharm Chemical Reagent Co., Ltd. (China). Ultrapure water obtained from a Millipore water purification system ($\geq$18 MΩ, Milli-Q, Millipore) was used in all assays. All other reagents were of analytical grade and used as received. Phosphate buffer solutions (PBS) were prepared by mixing the stock solutions of 0.05 M KH_2PO_4 and 0.05 M K_2HPO_4 containing 0.10 M KCl as the supporting electrolyte. The washing buffer (PBST) consisted of PBS (0.05 M, pH 7.4) and 0.05% (w/v) Tween 20, and the blocking solution was PBS (0.05 M, pH 7.4) containing 5% (w/v) BSA.

2.2. Apparatus

All electrochemical measurements were performed using a CHI630C electrochemical workstation (CH Instruments, Shanghai, China) with a conventional three-electrode system, which was constituted with a GCE as working electrode, a platinum wire as counter electrode and a Ag|AgCl (3.0 M KCl) as reference electrode. All electrodes were purchased from Gaoshiruilian Co., Ltd., Wuhan, China. Electrochemical impedance spectroscopy was carried out using an IM6ex electrochemical station (ZAHNER, Germany). The morphologies and chemical composition of the nano-materials were examined by scanning electron microscopy (SEM) and energy dispersive X-ray (EDX) (JSM-7500F, JEOL., Japan), transmission electron microscope (TEM, Tecnai G2 20, USA), Fourier transform infrared spectra (FT-IR, Nicolet 170, USA) and X-ray diffraction (XRD, X-PertPro, Netherland) with a Cu Kα radiation (λ=1.5406 nm). X-ray photoelectron spectra (XPS) were collected on an X-ray photoelectron spectrometer (ESCALAB 250Xi, USA) with a monochromated Al Kα source ($h\nu$=1486.6 eV), 150 W Power and 500 μm beam spot. The spectra were calibrated on the C1s peak (284.8 eV) and analyzed using XPSPEAK41 software.

2.3. Preparation of AuNPs|PANI|TNT composite

The preparation of AuNPs|PANI|TNT composite (Scheme 1A) referred a previous work with minor adjustment (Zhu et al., 2016). Initially, TNTs were prepared by delivering a mixture of 0.6 g TiO_2 nanoparticles and 120 mL (10 M) aqueous NaOH to a Teflon-lined autoclave for a hydrothermal reaction at 120 °C for 48 h. The obtained white crude product was washed alternately with 0.1 M HCl and water three times, and then adjusted with distilled water to achieve pH 7. During the hydrothermal process, the TiO_2 nanoparticles were firstly transferred into planar fragments after reacting with concentrated NaOH solution. A monolayer nanotube could then be obtained through the covalent bonding of the end groups of TiO_2 planar fragments. Finally, multilayer TiO_2 nanotubes were formed using the monolayer nanotube as a template.

The PANI|TNT composite was synthesized as follows: 0.2660 g of TNT were dispersed into a mixture of 8.57 mL aniline hydrochloride solution (0.1 M) and 10 mL HCl solution (0.1 M) in a reaction beaker and stirred with a magnetic stirrer in an ice water bath for half an hour to obtain a homogeneous suspension. Next, 8.57 mL APS hydrochloride solution (0.1 M) was added dropwise to the suspension over 2-h duration with continuous stirring at 0–5 °C. The resulting solution was allowed to react in ice bath for another 3 h and kept at room temperature over night. During the next day, the dark green precipitate was washed with Milli-Q water for several times until pH 7.0, dried in the vacuum oven at 60 °C for 3 h before it was grinded to powder.

The preparation of AuNPs|PANI|TNT composite was performed as follows: 1 mL $HAuCl_4$ (0.01 M) and 1 mL 0.01 M sodium citrate

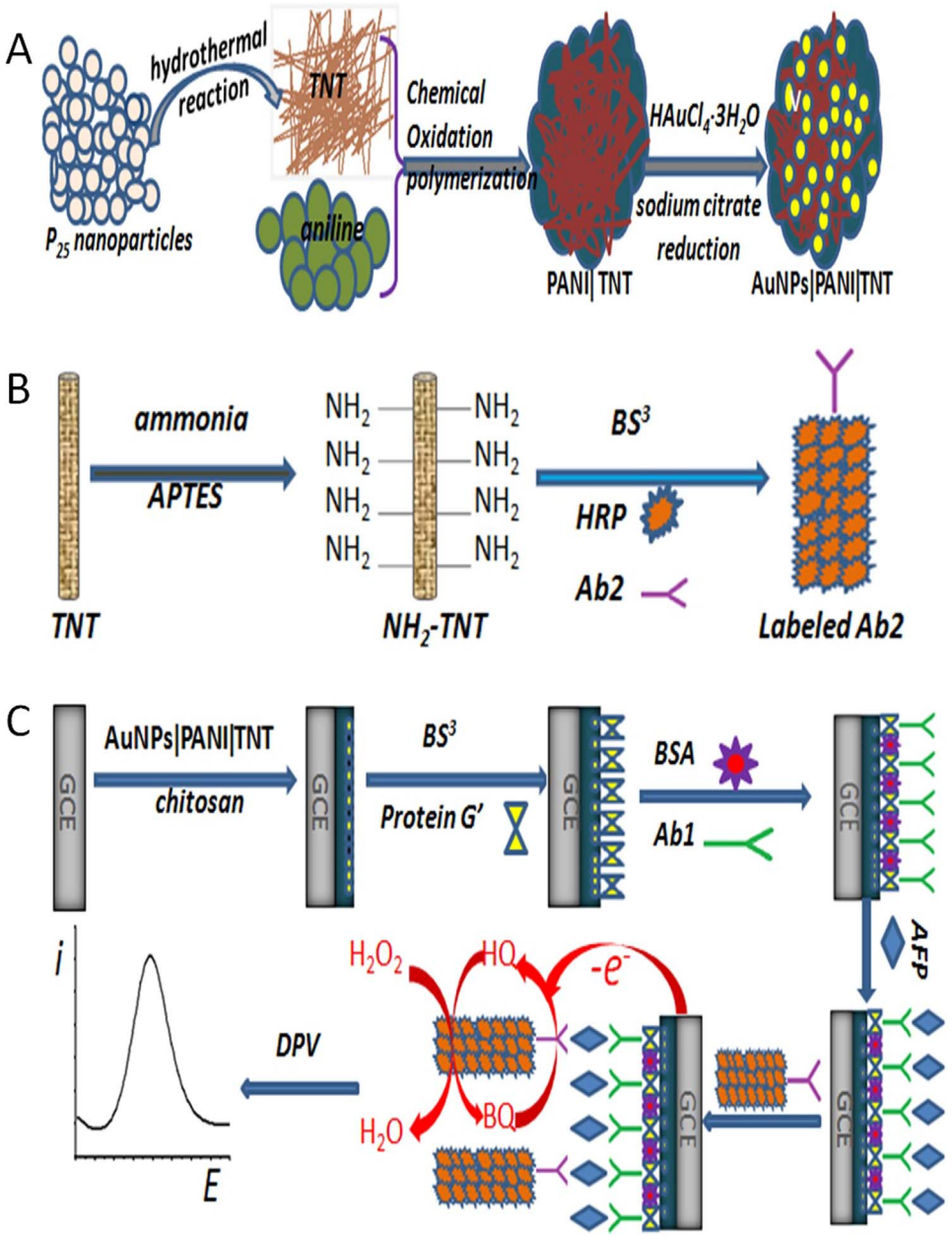

Scheme 1. Schematic illustration of preparation of (A) AuNPs|PANI|TNT composite, (B) HRP|NH_2-TNT|Ab2 bioconjugate and (C) immunosensor.

(capping agent) were added into a uniform suspension of 18 mg PANI|TNT in 18 mL Milli-Q water with continuous stirring. Next, 1 mL fresh $NaBH_4$ solution (0.1 M, 0–4 °C) was added to the suspension with vigorous stirring for 20 min. The suspension was then stirred for 0.5 h at room temperature before it was left undisturbed overnight. The composite was centrifuged and sequentially washed with Milli-Q water and ethanol, before it was dried in a 60 °C vacuum overnight.

2.4. Preparation of labeled signal antibody (Ab2)

The NH_2-TNTs were prepared according to the previous protocol with minor modification (Pearson et al., 2011). In brief, TNTs (100 mg) were added to a solution containing 20 mL ethanol, 1 mL ammonia (28%) and 4 mL APTES. The suspension was left overnight under mechanical stirring to prevent TNTs from settling. After the suspension was centrifuged, the supernatant was removed and the solid residue was washed three times with Milli-Q water. The amine-modified TNTs were then dried in oven at 60 °C and stored at room temperature for later use.

The preparation procedure of the HRP|NH_2-TNT|Ab2 bioconjugate was shown in Scheme 1(B). Firstly, 2 mg BS^3 was dissolved in 0.5 mL 0.02 M PBS (pH 7.4) and 3 mg NH_2-TNTs was then dispersed into BS^3 solution. Following that, the dispersion was incubated with 350 μL 2 mg mL^{-1} HRP for 30 min under proper stirring at room temperature. Afterward, 20 μL 0.6 mg mL^{-1} Ab2 was added into the mixture, followed by incubation at 4 °C for 4 h under gentle stirring. After centrifugation, the obtained bioconjugate was washed with PBS and then blocked with 2% BSA for 30 min at room temperature. Finally, the bioconjugate was washed with PBS again and suspended in 1.0 mL PBS containing 0.1% BSA.

2.5. Fabrication of immunosensor

The fabrication of the immunosensor was illustrated in Scheme 1 C. Briefly, 5 mg AuNPs|PANI|TNT composite was initially

dispersed in 1 mL 0.2% CS solution (in 0.2 M acetic acid) with 20 min sonification to obtain a homogeneous dispersion. Next, 5 μL of this suspension was cast on the pretreated GCE and dried at room temperature. A droplet (10 μL) of 2 mg mL^{-1} BS^3 solution was applied on the modified electrode and the electrode was left at room temperature for 1 h. Then 10 μL protein G′ (1 mg mL^{-1}) was immediately immobilized on the modified electrode, which was left at room temperature for another 1 h, followed by immersing the electrode in PBS for 3 min. After that, the electrode was exposed to 5 μL of 5% (w/v) BSA solution for 30 min to block possible remaining active sites against nonspecific adsorption and then washed with PBST and PBS respectively. Finally, 5 μL of 0.44 mg mL^{-1} capture antibody (Ab1) was incubated on the protein G′ modified electrode surface at room temperature for 1 h and the resulting modified electrode was then stored at 4 °C overnight in a 100% moisture-saturated environment. The as-prepared immunosensor was washed with PBST and PBS successively to remove the physically absorbed Ab1 and stored at 4 °C.

2.6. Electrochemical immunoassay procedure

To perform the immunoassay, the immunosensor was firstly incubated with 5 μL AFP solution for 50 min at room temperature, followed by PBST and PBS washing for 3 min successively. Next, it was incubated with 5 μL of labeled Ab2 for 50 min at room temperature and rinsed with PBST and PBS for 3 min respectively. Finally, the immunosensor, Ag|AgCl reference electrode and Pt counter electrode were placed in an electrochemical cell containing 10 mL PBS. Prior to the experiments, the test solution was deoxygenized by high purity nitrogen for 15 min and maintained in nitrogen atmosphere during the detection. Hydroquinone (final concentration 2 mM) and H_2O_2 (final concentration 1 mM) were then injected in the cell and differential pulse voltammetry (DPV) was scanned from 0.2 to −0.2 V (vs Ag/AgCl) with a pulse amplitude of 50 mV and a pulse width of 50 ms for quantitative detection of AFP.

3. Results and discussion

3.1. Characterization of TNTs, PANI|TNT and AuNPs|PANI|TNT composite

The microscopic images of TNT, PANI|TNT and AuNPs|PANI|TNT composite and EDX pattern of the ternary composite were displayed to characterize their morphologies and confirm the formation of the ternary composite (Fig. 1). The prepared TNTs showed the elongated tubular morphology with a length up to

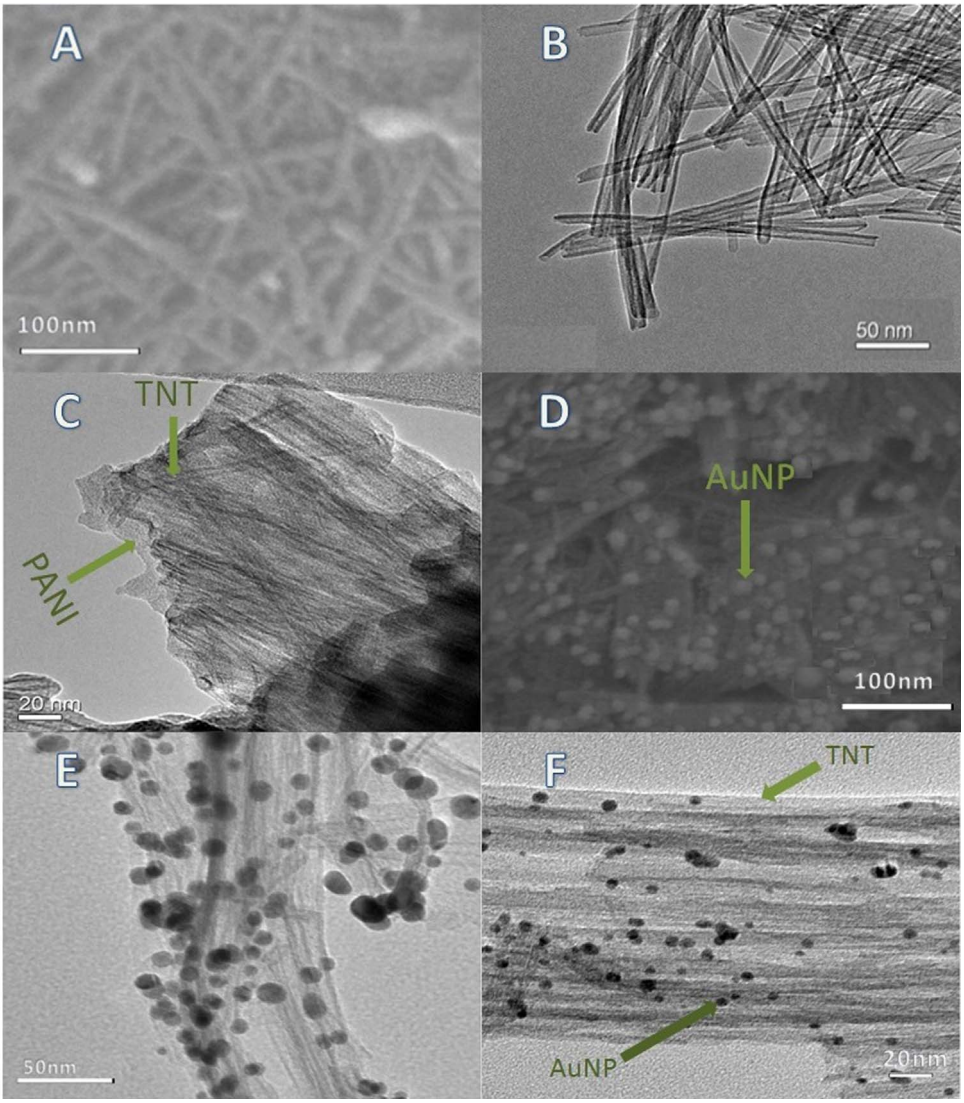

Fig. 1. SEM images of (A) TNTs and (D) AuNPs|PANI|TNT composite; TEM images of (B) TNTs, (C) PANI|TNT, (E) AuNPs|PANI|TNT and (F) AuNPs|TNT composite.

several hundred nm and a diameter between 8 and 13 nm (Fig. 1A). The TEM image of TNTs also demonstrated that TNTs possessed long tubular structure with comparable diameter size with biomolecules (Fig. 1B), which could be immobilized by biomolecules and used as tracing tag in electrochemical immunosensor. Moreover, no obvious granular particles of P25 were observed in Fig. 1A and B, indicating that the TiO_2 nanoparticles had been completely transformed into TiO_2 nanotubes. After the chemical oxidation polymerization of aniline on TNTs, the TEM of PANI|TNT composite displayed the coating of semi-transparent PANI on TNTs (Fig. 1C), and a lot of spherical particles were observed on the surface of PANI|TNT composite without any significant agglomeration (Fig. 1D), indicating the reduction deposition of AuNPs on PANI|TNT. The TEM images of AuNPs|PANI|TNT (Fig. 1E) and AuNPs|TNT (Fig. 1F) demonstrated that the density of AuNPs on PANI|TNT was much larger than that on pure TNTs (Liu et al., 2013), which is probably due to the adsorption of $AuCl_4^-$ to the positive charged amino groups on PANI (Liu et al., 2012). From the SEM and TEM graphs, the average particle size of Au was estimated to be ~15 nm. EDX analysis was also performed to investigate the elemental composition of the AuNPs|PANI|TNT composite (Fig. S1), which demonstrated the successful immobilization of AuNPs on PANI|TNT surface to form a ternary composite.

3.2. XPS characterization and X-ray diffraction pattern of AuNPs|PANI|TNT composite

The XPS measurements were also conducted to investigate the elemental composition of the ternary composite. The XPS survey spectrum of AuNPs|PANI|TNT contains Ti2p, O1s, C1s, N1s, Au4d and Au4f peaks (Fig. 2A), which belong to the typical elements existing in the composite (Yan et al., 2016; Zhou et al., 2013). The XPS high-resolution spectrum of Ti2p showed two peaks centered at 458.8 and 464.5 eV, assigned to $Ti2p_{3/2}$ and $Ti2p_{1/2}$ respectively (Sim et al., 2015; Yang et al., 2014) (Fig. 2B). The XPS spectrum of O1s (Fig. 2C) displayed another two peaks at 532.2 and 530.5 eV,

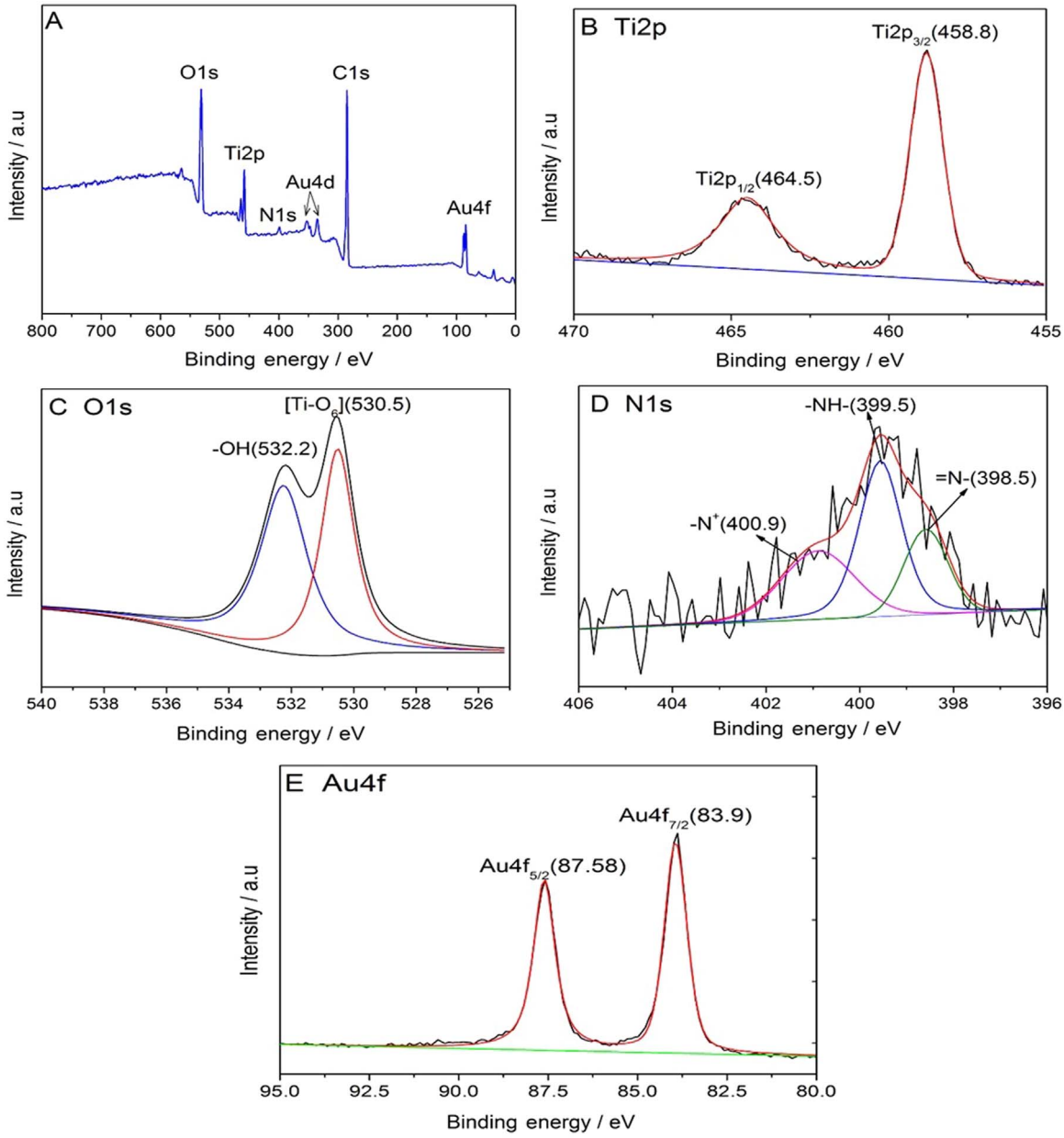

Fig. 2. XPS analysis of AuNPs|PANI|TNT composite. (A) XPS survey scans, and high-resolution XPS spectra of (B) Ti2p, (C) O1s, (D) N1s and (E) Au4f.

which were attributed to the O from TNT surface Ti-OH groups and the lattice oxygen [Ti-O_6] in TNTs (X. Li et al., 2015; Yang et al., 2014). The existence of both Ti2p and O1s peaks confirmed the successful preparation of TNTs. The high-resolution N1s spectrum of AuNPs|PANI|TNT composite could be fitted into three peaks centered at 398.5 eV, 399.5 eV and 400.9 eV respectively, which corresponded to three different nitrogen environments (Fig. 2D). The lower binding energy peaks at 398.5 eV and 399.5 eV were ascribed to the quinonoid imine (=N–) and benzenoid amine (–NH–) in PANI (P. Wang et al., 2014; Yang et al., 2014), the other peak with binding energy at 400.9 eV was assigned to protonated amine or positively charged nitrogen (-N^+) (Yang et al., 2014). As reported previously, the N peak at 400.9 eV indicated that PANI was in a highly conductive state with good electron transfer capability (Yang et al., 2014). The $Au4f_{7/2}$ and $Au4f_{5/2}$ spin-orbital splitting photoelectron spectrums located at 83.9 and 87.58 eV corresponded well to the standard binding energy of Au (84.0 and 87.6 eV) (Yang et al., 2014) (Fig. 2(E)), implying that AuNPs were successfully deposited on PANI|TNT by chemical reduction of $HAuCl_4$. Similarly, after GNPs were deposited on the TNT-PANI surface, the X-ray diffraction pattern of AuNPs|PANI|TNT composite showed not only the peaks ascribed to TNT-PANI composite, but also the peaks attributed to gold nanoparticles (Fig. S2).

3.3. FT-IR characterization of TNTs, NH_2-TNTs, PANI, PANI|TNT and AuNPs|PANI|TNT composite

The structural information of the materials prepared in this work was investigated by FT-IR technique (Fig. 3A). TNTs displayed a broad absorption from 3000 to 3700 cm^{-1} and a sharp peak at 1631 cm^{-1} from the surface hydroxyl vibration (Zhang et al., 2009) (Fig. 3A, curve a). In addition, another characteristic absorption band (400–700 cm^{-1}) originated from the Ti–O stretching and Ti-O-Ti bridging vibration of TiO_2 nano-materials was also observed on Fig. 3A, curve a. After the amination of TNTs, two obvious peaks at 1625 cm^{-1} and 1508 cm^{-1} assigned to N-H bending vibration peaks of the primary amine (-NH_2) groups were observed (Li et al., 2014) (Fig. 3A, curve b). The peak at 1625 cm^{-1} (Fig. 3A, curve b) is noticeably larger than that at 1631 cm^{-1} from the adsorbed water molecules (Fig. 3A, curve a). However, the stretching vibration band of the primary amine group between 3400 and 3500 cm^{-1} was overlapped with the O-H stretching band of TNTs (Lin et al., 2016) (Fig. 3A, curve b). PANI displayed some typical peaks at 1299, 1125 and 797 cm^{-1}, which were ascribed to the C–N stretching of the secondary aromatic amine, the N=Q=N (Q represents the quinoid ring) stretching and the aromatic C-H out-of-plane bending vibration respectively (Karim et al., 2009) (Fig. 3A, curve c). In addition, the peaks at 1563 cm^{-1} and 1474 cm^{-1} were ascribed to the C=C stretching vibration of quinoid and benzenoid rings in PANI (Irimia-Vladu et al., 2008). More importantly, the peak at 1242 cm^{-1} due to the C-$N^{+\bullet}$ stretching vibration suggested that PANI was in the form of a conductive emeraldine salt (ES) (Oh and Kim, 2012). The PANI/TNT composite showed both the characteristic bands of PANI (700–1600 cm^{-1}) and the absorption band attributable to Ti–O–Ti and Ti-O vibration (400–700 cm^{-1}) (Fig. 3A, curve d). Noticeably, upon the coating of PANI on TNT, the characteristic PANI absorption peaks at 1563, 1474, 1299 and 1125 cm^{-1}, corresponding to the stretching mode of C=C, C–N and N=Q=N bands, respectively shifted to 1574, 1489, 1305 and 1145 cm^{-1}, which could be attributed to the strong interaction between nitrogen atoms in PANI and titanate. AuNPs|PANI|TNT composite also exhibited both the characteristic bands of PANI and the absorption bands attributable to Ti-O-Ti and Ti-O vibration, while AuNPs did not show any notable FT-IR absorption (Fig. 3A, curve e). Due to the strong interaction between AuNPs and PANI, the deposition of AuNPs on PANI-TNT composite resulted in further shift of characteristic PANI absorption peaks to 1580, 1503, 1309 and 1147 cm^{-1} respectively.

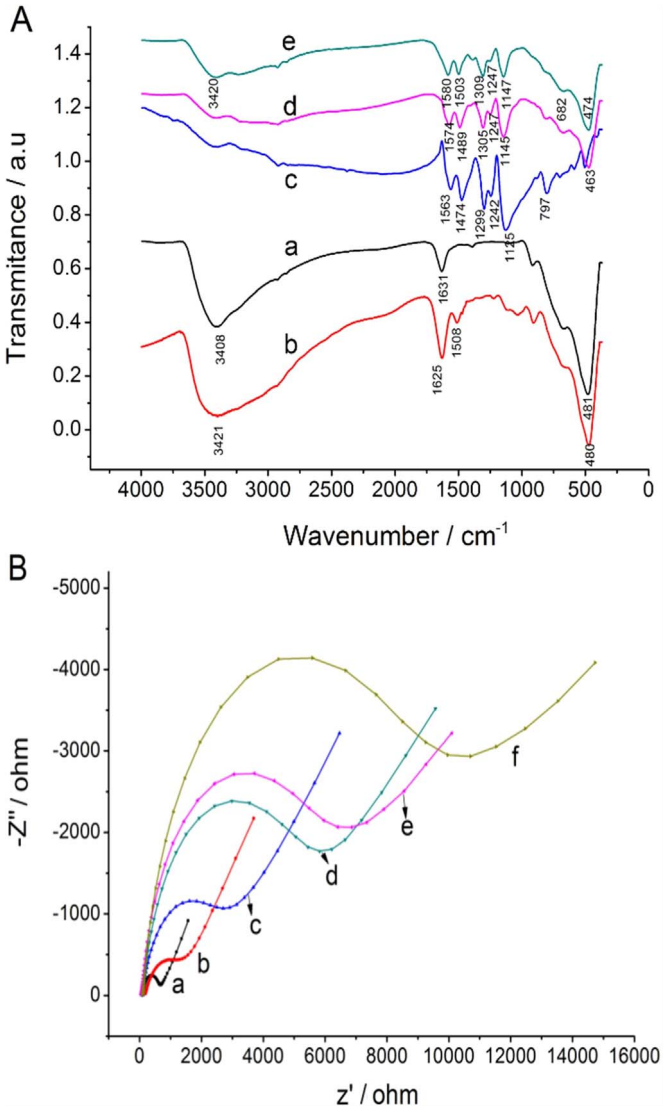

Fig. 3. (A) FT-IR spectra of (a) TNTs, (b) NH_2-TNTs, (c) PANI, (d) PANI|TNT and (e) AuNPs|PANI|TNT composite; (B) Nyquist plots of (a) bare GCE, (b) AuNPs|PANI|TNT|chitosan, (c) AuNPs|PANI|TNT|chitosan|protein G′, (d) AuNPs|PANI|TNT|chitosan|protein G′|BSA, (e) AuNPs|PANI|TNT|chitosan|protein G′|BSA|Ab1 and (f) AuNPs|PANI|TNT|chitosan|protein G′|BSA|Ab1|AFP|labeled Ab2 modified GCE.

3.4. EIS investigation on assembly process of the immunosensor

Electrochemical impedance spectroscopy (EIS) is an effective tool to evaluate the process kinetics and interfacial properties of the modified electrodes. Therefore, EIS was used to probe the stepwise assembly of the AFP immunosensor fabricated in this work. The specific construction process of the immunosensor was illustrated in Scheme 1 C. Impedance experiments were performed in 5 mM $K_3[Fe(CN)_6]|K_4[Fe(CN)_6]$ containing 0.1 M KCl at a DC potential of 0.21 V superimposed by an alternating voltage of 5 mV. Nyquist plots were recorded over a frequency range from 50 kHz to 100 mHz. As shown in Fig. 3B and Fig. S3, all the Nyquist plots included a semicircular portion at high frequency region corresponding to the electron transfer resistance (R_{et}) and a linear portion at low frequency region controlled by the diffusion process. The semicircular diameter is proportional to the R_{et} of $K_3[Fe(CN)_6]|K_4[Fe(CN)_6]$ at the modified electrode surface (Zhang

et al., 2015). As expected, the bare GCE displayed a very small semicircle, indicating a small R_{et} at the surface and thus a nearly diffusion-controlled process (Fig. 3B, curve a). From curve b to f, the bare GCE was successively modified with the ternary composite-chitosan dispersion, Protein G′, BSA, capture antibody and signal antibody. Accordingly, the semicircle diameter increased gradually with the stepwise modification process, indicating that the electron transfer rate was decreased due to the immobilization materials on the GCE. The immobilized nanomaterials and biomolecules formed a barrier layer on the electrode surface, which could obstruct the electron transfer and therefore increased the R_{et}. These results demonstrated that the materials were successfully immobilized on the electrode surface.

3.5. Optimization of immunoassay conditions

The amperometric response of the immunosensor to AFP depended on the preparation of both the immunosensor and the tracer label. The response increased dramatically with the increasing concentration of Ab1, and reached a platform at 0.44 mg mL^{-1}, then decreased slightly when the Ab1 concentration was over 1 mg mL^{-1} (Fig. 4A). The higher concentration of Ab1 could connect more AFP on sensor surface, however, it also produced space hinder to reduce the binding of tracer labels. The ratio of HRP to Ab2 on TNTs was optimized to be 35:2 (Fig. 4B). The pH value of the test solution significantly affected the enzymatic reaction. The optimal test solution was 0.05 M PBS (pH 7.0) containing 0.10 M KCl (Fig. S4A). The incubation time of AFP on the immunosensor was optimized to be 50 min (Fig. S4B).

3.6. Analytical performance of the immunosensor

HRP has been widely used as a signal amplification label in electrochemical immunoassay due to its stability, high catalytic capability and ultra-sensitivity. At the TNT-PANI-GNP modified GCE, the immobilized HRP showed an irreversible reduction peak at ~ -0.15 V due to the direct electron transfer of HRP (Fig. S5). The excellent conductivity and biocompatibility of GNPs, as well as the high loading of HRP, led to higher reduction current at the modified electrode than that in the absence of GNPs. After HRP molecules and capture antibody were immobilized on TNTs through BS^3 to form a tracing tag for the detection of AFP, HRP could catalyze the conversion of hydroquinone to benzoquinone with the assistance of H_2O_2, which was then reduced back to hydroquinone to generate an electrochemical detection signal.

Under the optimum conditions, DPV was used to investigate the analytical performance of the immunosensor. As shown in Fig. 4C, the reduction peak currents increased with the increasing of AFP concentration, based on which a calibration plot was plotted as the inset. The calibration plot showed good linear relationship between the peak currents and the logarithm of AFP concentration in a concentration range from 0.01 to 350 ng mL^{-1} with a correlation coefficient of 0.994 ($n=8$). The detection limit of the immunosensor was estimated to be 1.5 pg mL^{-1} at a signal-to-

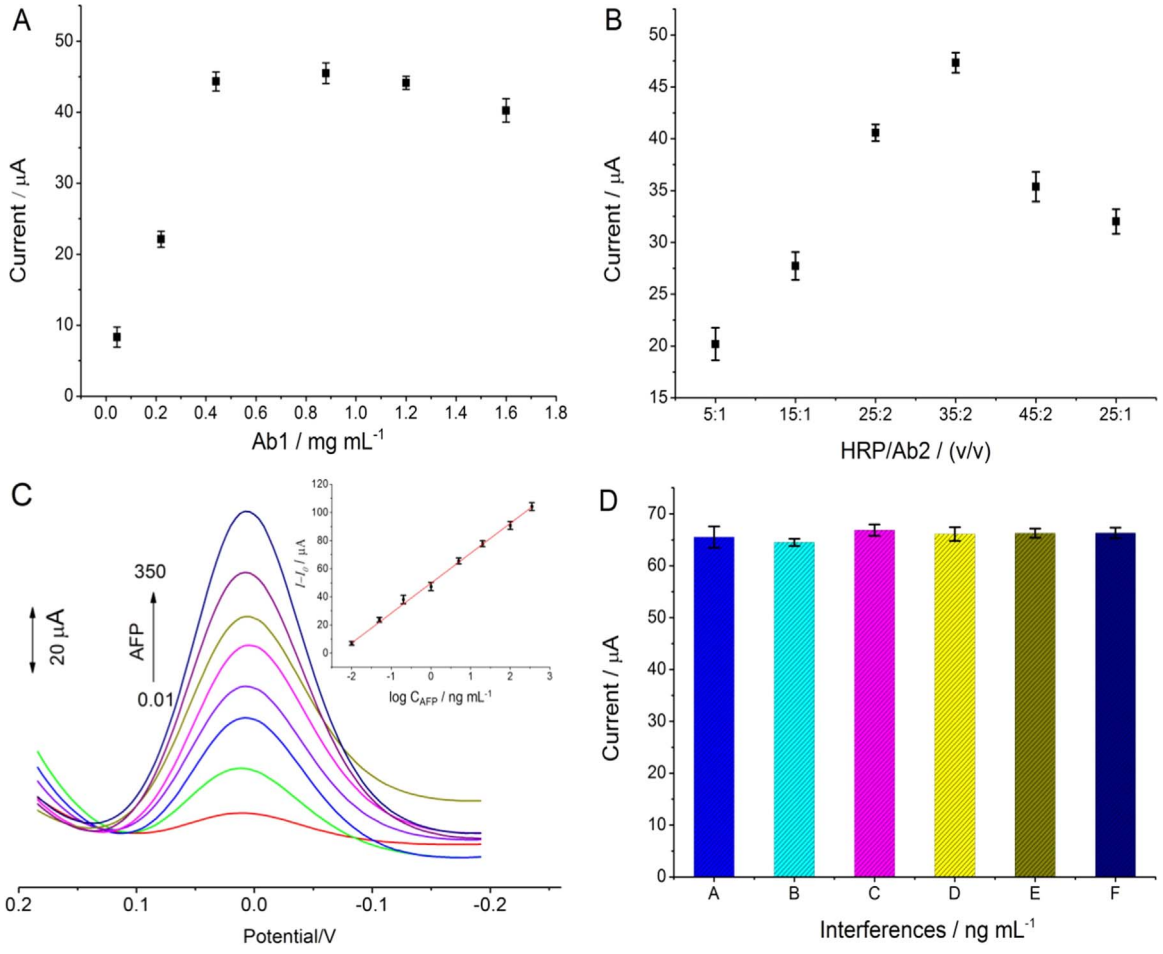

Fig. 4. Effects of (A) Ab1 concentration and (B) ratio of HRP to Ab2 on DPV response of the proposed immunosensor; (C) DPV responses of the proposed immunosensor to increasing concentration of AFP from 0.01 to 350 ng mL^{-1}. Inset: Plot of DPV response versus logarithms of AFP concentration. (D) Specificity of the immunosensor to (a) 5 ng mL^{-1} AFP, (b) 5 ng mL^{-1} AFP +100 ng mL^{-1} CEA, (c) 5 ng mL^{-1} AFP +100 ng mL^{-1} PSA, (d) 5 ng mL^{-1} AFP +100 ng mL^{-1} CA125, (e) 5 ngmL^{-1} AFP +100 ng mL^{-1} IgG and (f) 5 ngmL^{-1} AFP +100 ng mL^{-1} BSA.

Table 1.
Comparison of the proposed immunosensor with other sensors for AFP detection.

Immunosensors	Linear range (ng mL^{-1})	Limit of detection (pg mL^{-1})	References
CS-AuNPs/Ab1/AFP/CuNCs[a] -Au-Ab2	0.025–250	10.9	(Z. Wang et al., 2014)
Pd-rGO[b]/Ab1/BSA/AFP	0.01–12	5	(Qi et al., 2014)
GS[c]-Thi[d]/Ab1/AFP/PB@HAP[e] -HRP-Ab2	0.02–8	9	(Dai et al., 2011)
CNPs[f]-CS- Ab1/AFP/ Ab2- ISNG[g]- HRP	0.02–4	10	(Tang et al., 2010)
Au-Fe_3O_4/Ab2/AFP/Ab1/Au/chitosan/GCE	0.01–40	2.3	(Parshetti et al., 2013)
Nafion-Protein A-Ab1/AFP/Thi @Ab2-PTCA[h]/Au/GS	0.016–50	5.4	(Zhu et al., 2013)
CD[i]-GS/Ab1/AFP/Ab2-Pt@CuO -MWCNTs-Ab2	0.001–20	0.33	(Jiang et al., 2015)
AuNPs|PAN|TNT|chitosan|proteinG'| Ab1|AFP|labeled Ab2	0.01–350	1.5	This work

[a] $Cu_3[Co(CN)_6]_2$.
[b] Reduced graphene oxide.
[c] Graphene sheet.
[d] Thionine.
[e] Prussian blue@hydroxyapatite.
[f] Carbon nanoparticles.
[g] Irregular-shaped gold nanoparticles.
[h] 3,4,9, 10-perylene tetracarboxylic acid.
[i] β–cyclodextrin.

noise ratio of 3. As presented in Table 1, this immunosensor showed superiority over most of the other AFP immunosensors in analytical performance owing to the excellent biocompatibility and conductivity of AuNPs|PANI|TNT, oriented binding capability of Protein G′ and strong signal amplification of TNT tracing tag.

3.7. Specificity, precision, stability and practical application of the immunosensor

To evaluate the selectivity of the immunosensor, several possible interferences including carcinoembryonic antigen (CEA), prostate protein antigen (PSA), carcinoma antigen 125 (CA125), immunoglobulin G (IgG) and BSA were introduced. The immunosensor was incubated with a solution of 5 ng mL^{-1} AFP containing one of the above interferences (100 ng mL^{-1}). The current variation due to the interfering substances was less than 5% of the current signal in the absence of the interferences (Fig. 4D), demonstrating the good selectivity of the immunosensor. The reproducibility of the immunosensor was investigated by measuring the same sample with five electrodes prepared independently in the identical experimental conditions. A relative standard deviation (RSD) of 5.2% was obtained, suggesting the acceptable precision of the proposed immunoassay.

The stability of the immunosensor was also examined by detecting the responses every two days for two weeks. The signal retained 93.2% of the initial signal after two weeks, indicating acceptable good stability. The signals for six measurements of AFP sample gave a RSD of 3.6%, showing good repeatability of the measurements. After AFP of 0.1, 1 and 10 ng mL^{-1} was spiked into serum samples, the immunosensor showed the recovery of 96.4–105.1%, indicating that the immunosensor could be potentially applied in the clinical detection of AFP.

4. Conclusion

AuNPs|PANI|TNT composite was synthesized through chemical oxidation polymerization of aniline on TNTs and following chemical reduction deposition of AuNPs on PANI|TNT. SEM, TEM, EDX, XPS, XRD and FT-IR characterization evidenced the formation of the ternary composite. EIS results were used to monitor the assembly process of the immunosensor. More specifically, protein G' was bound on AuNPs|PANI|TNT|chitosan for oriented immobilization of capture antibody, and the TNT was also functionalized with signal antibody and HRP to produce a tracing tag. The immunosensor showed a wide linear range with a detection limit of 1.5 pg mL^{-1}. The performance was better than many reported AFP immunosensors due to the good electrical conductivity and high specific surface area of AuNPs|PANI|TNT, great signal amplification effect of tracing tag, and the inherent property of protein G′ for oriented immobilization of an enhanced quantity of capture antibody. The immunosensor assembly could be extended to other labeled recognition systems and provided good stability, reproducibility and accuracy for potential applications in bioanalysis and clinical diagnostics.

Acknowledgments

This work was financially supported by the Open Research Funding of State Key Laboratory of Analytical Chemistry for Life Science, Nanjing University (No. SKLACLS1409), National Natural Science Foundation of China (No. U1504215) and the Scientific Research Foundation for the Returned Overseas Chinese Scholars, State Education Ministry (Batch 46th).

Appendix A. Supplementary material

Supplementary data associated with this article can be found in the online version at http://dx.doi.org/10.1016/j.bios.2016.05.053.

References

Chang, Y.-F., Chen, R.-C., Lee, Y.-J., Chao, S.-C., Su, L.-C., Li, Y.-C., Chou, C., 2009. Biosens. Bioelectron. 24, 1610–1614.
Chou, S.-F., Hsu, W.-L., Hwang, J.-M., Chen, C.-Y., 2002. Clin. Chem. 48, 913–918.
Dai, Y., Cai, Y., Zhao, Y., Wu, D., Liu, B., Li, R., Yang, M., Wei, Q., Du, B., Li, H., 2011. Biosens. Bioelectron. 28, 112–116.
Ekins, R., 1999. J. Clin. Immunoass. 22, 61–77.
Fowler, J.M., Stuart, M.C., Wong, D.K.Y., 2007. Biosens. Bioelectron. 23, 633–639.
Goward, C.R., Murphy, J.P., Atkinson, T., Barstow, D.A., 1990. Biochem. J. 267, 171–177.
Irimia-Vladu, M., Marjanovic, N., Vlad, A., Ramil, A.M., Hernandez-Sosa, G., Schwoödiauer, R., Bauer, S., Sariciftci, N.S., 2008. Adv. Mater. 20, 3887–3892.
Jiang, L., Han, J., Li, F., Gao, J., Li, Y., Dong, Y., Wei, Q., 2015. Electrochim. Acta 160, 7–14.
Karim, M.R., Lim, K.T., Lee, M.S., Kim, K., Yeum, J.H., 2009. Synth. Met. 159, 209–213.
Kavosi, B., Hallaj, R., Teymourian, H., Salimi, A., 2014. Biosens. Bioelectron. 59, 389–396.
Li, F., Han, J., Jiang, L., Wang, Y., Li, Y., Dong, Y., Wei, Q., 2015. Biosens. Bioelectron. 68, 626–632.
Li, N., Ma, H., Cao, W., Wu, D., Yan, T., Du, B., Wei, Q., 2015. Biosens. Bioelectron. 74, 786–791.
Li, P., Zhang, B., Cui, T., 2015. Biosens. Bioelectron. 72, 168–174.

Li, S., Zhai, S.-R., An, Q.-D., Li, M.-H., Song, Y., Song, X.-W., 2014. Mater. Res. Bull. 60, 665–673.
Li, X., Liu, W., Ni, J., 2015. Microporous Mesoporous Mater. 213, 40–47.
Liang, W.-B., Yuan, R., Chai, Y.-Q., Li, Y., Zhuo, Y., 2008. Electrochim. Acta 53, 2302–2308.
Lin, K.-Y.A., Liu, Y.-T., Chen, S.-Y., 2016. J. Colloid Interface Sci. 461, 79–87.
Liu, J., Lin, G., Xiao, C., Xue, Y., Yang, A., Ren, H., Lu, W., Zhao, H., Li, X., Yuan, Z., 2015. Biosens. Bioelectron. 71, 82–87.
Liu, S., Xu, H., Ou, J., Li, Z., Yang, S., Wang, J., 2012. Mater. Chem. Phys. 132, 500–504.
Liu, S., Yuan, R., Chai, Y., Su, H., 2011. Sens. Actuators, B 156, 388–394.
Liu, X., Zhang, J., Liu, S., Zhang, Q., Liu, X., Wong, D.K.Y., 2013. Anal. Chem. 85, 4350–4356.
Luppa, P.B., Sokoll, L.J., Chan, D.W., 2001. Clin. Chim. Acta 314, 1–26.
Maeng, J.-H., Lee, B.-C., Ko, Y.-J., Cho, W., Ahn, Y., Cho, N.-G., Lee, S.-H., Hwang, S.Y., 2008. Biosens. Bioelectron. 23, 1319–1325.
Meusel, M., Renneberg, R., Spener, F., Schmitz, G., 1995. Biosens. Bioelectron. 10, 577–586.
Oh, M., Kim, S., 2012. Electrochim. Acta 78, 279–285.
Paradela, A., Albar, J.P., 2008. J. Proteome Res. 7, 1809–1818.
Parshetti, G.K., Lin, F.-h., Doong, R.-a., 2013. Sens. Actuators, B 186, 34–43.
Pearson, A., Jani, H., Kalantar-zadeh, K., Bhargava, S.K., Bansal, V., 2011. Langmuir 27, 6661–6667.
Pinwattana, K., Wang, J., Lin, C.-T., Wu, H., Du, D., Lin, Y., Chailapakul, O., 2010. Biosens. Bioelectron. 26, 1109–1113.
Qi, T., Liao, J., Li, Y., Peng, J., Li, W., Chu, B., Li, H., Wei, Y., Qian, Z., 2014. Biosens. Bioelectron. 61, 245–250.
Qin, G., Zhao, S., Huang, Y., Jiang, J., Ye, F., 2012. Anal. Chem. 84, 2708–2712.
Sim, L.C., Leong, K.H., Saravanan, P., Ibrahim, S., 2015. Appl. Surf. Sci. 358, 122–129.
Song, Y.-Y., Zhuang, Q.-L., Li, C.-Y., Liu, H.-F., Cao, J., Gao, Z.-D., 2012. Electrochem. Commun. 16, 44–48.
Staros, J.V., 1982. Biochemistry 21, 3950–3955.
Tang, J., Su, B., Tang, D., Chen, G., 2010. Biosens. Bioelectron. 25, 2657–2662.
Thamake, S.I., Raut, S.L., Ranjan, A.P., Gryczynski, Z., Vishwanatha, J.K., 2011. Nanotechnology 22, 35101–35110.
Wang, G.-L., Xu, J.-J., Chen, H.-Y., Fu, S.-Z., 2009. Biosens. Bioelectron. 25, 791–796.
Wang, P., Du, M., Zhang, M., Zhu, H., Bao, S., Zou, M., Yang, T., 2014. Chem. Eng. J. 248, 307–314.
Wang, Z., Chen, X., Ma, Z., 2014. Biosens. Bioelectron. 61, 562–568.
Xu, R., Jiang, Y., Xia, L., Zhang, T., Xu, L., Zhang, S., Liu, D., Song, H., 2015. Biosens. Bioelectron. 74, 411–417.
Yan, M., Shen, Y., Zhang, G., Bi, H., 2016. Mater. Sci. Eng. C. 58, 568–575.
Yang, K., Huang, K., He, Z., Chen, X., Fu, X., Dai, W., 2014. Appl. Catal. B 158–159, 250–257.
Zhang, H., Lv, X., Li, Y., Wang, Y., Li, J., 2009. ACS Nano 4, 380–386.
Zhang, J.-J., Kang, T.-F., Hao, Y.-C., Lu, L.-P., Cheng, S.-Y., 2015. Sens. Actuators B 214, 117–123.
Zhao, L., Wei, Q., Wu, H., Dou, J., Li, H., 2014. Biosens. Bioelectron. 59, 75–80.
Zhou, X., Shi, T., Wu, J., Zhou, H., 2013. Appl. Surf. Sci. 287, 359–368.
Zhu, Q., Chai, Y., Yuan, R., Zhuo, Y., Han, J., Li, Y., Liao, N., 2013. Biosens. Bioelectron. 43, 440–445.
Zhu, J., Huo, X., Liu, X., Ju, H., 2016. ACS Appl. Mater. Interfaces 8, 341–349.